MIT Libraries | DSpace@MIT

MIT Open Access Articles

Tunable Raman spectroscopy study of CVD and peapod-derived bundled and individual double-wall carbon nanotubes

Massachusetts Institute of Technology

Tunable Raman spectroscopy study of CVD and peapod-derived bundled and individual double-wall carbon nanotubes

F. Villalpando-Paez,[1] L. G. Moura,[2] C. Fantini,[2] H. Muramatsu,[3] T. Hayashi,[3] Y. A. Kim,[3] M. Endo,[3] M. Terrones,[4] M. A. Pimenta,[2] and M. S. Dresselhaus[5]

[1]*Department of Materials Science and Engineering, Massachusetts Institute of Technology, Cambridge, Massachusetts 02139-4307, USA*

[2]*Departamento de Física, Universidade Federal de Minas Gerais, Belo Horizonte, Minas Gerais, Brazil*

[3]*Faculty of Engineering, Shinshu University, 4-17-1 Wakasato, Nagano-shi 380-8553, Japan*

[4]*Department of Materials Science and Engineering and Chemical Engineering, Carlos III University of Madrid,*
Avenida Universidad 30, 28911 Legans, Madrid, Spain
and Exotic Nanocarbon Research Center, Shinshu University, 4-17-1 Wakasato, Nagano city 380-8553, Japan

[5]*Department of Physics and Department of Electrical Engineering and Computer Science, Massachusetts Institute of Technology,*
Cambridge, Massachusetts 02139-4307, USA

We use 40 laser excitation energies to analyze the differences in the Raman spectra from chemical vapor deposition-derived double-wall carbon nanotube (CVD-DWNT) bundles, fullerene-derived DWNT bundles (C_{60}-DWNTs), and individual fullerene-derived DWNTs with inner type-I and type-II semiconducting tubes paired with outer metallic tubes. For the radial breathing mode (RBM) of SWNTs, an experimental ω_{RBM} vs d_t relationship of the form $\omega_{RBM}=A/d_t+B$ is obtained for the inner tubes of DWNT bundles where the A and B constants are found to be close to those obtained by elasticity theory when modeling the elastic properties of graphite. A similar change in ω_{RBM} is observed for an inner type-II semiconducting (6,5) tube and a type-I (9,1) tube when inside various metallic outer tubes. The G-band frequency is observed to upshift when switching the laser resonance from DWNTs with semiconducting inner tubes to DWNTs with metallic inner tubes. Finally, we measure the G′ feature from C_{60}-DWNTs and note a downshift in frequency with respect to that of CVD-DWNTs.

PACS number(s): 63.22.−m, 63.22.Gh, 81.07.De

I. INTRODUCTION

Double-wall carbon nanotubes (DWNTs) are of scientific interest because they provide the simplest system in which to study the interaction between two concentric carbon nanotubes. Furthermore, the inner and outer tubes of a DWNT can be either metallic (M) or semiconducting (S) so that four different configurations of DWNTs are possible (M@M, S@S, M@S, and S@M). The electronic and optical properties of a DWNT are dependent on the individual properties of its constituent inner and outer tubes and on intertube interactions. Since different DWNT synthesis processes yield different inner-outer tube pairs, the electronic and optical properties of current DWNT samples are highly dependent on the fabrication procedure. The two main fabrication procedures used to synthesize DWNTs include the following: (a) chemical vapor deposition (CVD) (DWNTs)[1] or (b) the filling of SWNTs with fullerenes where a second inner tube is created by heat-induced coalescence of the fullerenes (C_{60}-DWNTs).[2,3] The CVD-DWNTs and C_{60}-DWNTs have been reported to have some differences in their electronic and optical properties due to differences in the crystallinity of the resulting inner tubes and in the characteristic distance between the inner and outer tubes.[4] For instance, C_{60}-DWNTs have been observed to have smaller average wall to wall distances (defined as the distance between the inner and outer walls of the DWNT) than CVD-DWNTs for DWNTs with similar inner diameters. Also, the photoluminescence (PL) emission from the inner tubes of DWNTs appears to be highly dependent on sample fabrication and purity because both high and low intensity PL signals from the inner tubes of DWNTs have been reported for CVD-DWNTs[5] and C_{60}-DWNTs,[6] respectively. The fact that current DWNT synthesis procedures yield samples that contain a mixture of DWNTs with all four of the configurations listed above further complicates Raman data analysis because the Raman spectra from DWNT bundles contain contributions from most of the four possible DWNT configurations. Thus, it is difficult to quantitatively determine the actual (n,m) indices of the constitutive inner-outer tube pairs present in a DWNT bundle. In an effort to study DWNTs with a known configuration, we have performed tunable Raman experiments on DWNT bundles and complemented these studies with careful studies at the individual DWNT nanotube level capable of finding Raman resonances with both the inner and outer tubes of the same DWNT. Herein, we analyze the differences between the Raman spectra obtained from CVD-derived and C_{60}-derived DWNT bundles with 40 laser excitation energies. We also compare the radial breathing mode (RBM) features from individual DWNTs with the RBM features from DWNT bundles.

II. EXPERIMENTAL DETAILS

We used a CVD method to synthesize the CVD-DWNT bundles used in this study.[1] In order to remove unwanted catalyst residues, the sample was heat treated in an HCl solution at 100 °C for 10 h. Also, since DWNTs can withstand higher heat treatment temperatures than SWNTs, oxidation in air at 500 °C for 30 min was used to remove amorphous

carbon and impurities in the form of SWNTs. The high purity of our CVD-DWNT bundles relative to residual catalyst particles was confirmed by diamagnetic susceptibility measurements,[7] and the purity with regard to the absence of SWNTs was confirmed by transmission electron microscopy studies.[8,9] The C_{60}-DWNT bundles used herein were fabricated by reacting C_{60} and SWNTs under vacuum conditions at 600 °C for 24 h. The starting SWNT material was synthesized by the arc method and purified by Hanwha Corporation (Korea). The as-grown peapods (SWNTs containing encapsulated C_{60} fullerenes) were washed with toluene to remove residual C_{60} and heat treated at 1700 °C in Ar (1 atm) to transform them into C_{60}-DWNT bundles. The individual C_{60}-DWNTs were obtained by dispersing 1 mg of C_{60}-DWNTs in D_2O with 0.5 wt % sodium dodecilbenzene-sulfonate and sonicating the dispersion (600 W cm^{-2}) for 15–30 min. The solution was then ultracentrifuged (320 000 g) for 30 min, and 70% of the supernatant solution was collected. The supernatant solution containing the isolated C_{60}-DWNTs was spin coated on a Si chip with gold markers, and a Raman mapping technique described elsewhere[10] was used to obtain Raman resonance spectra from the inner and outer layers of the same individual DWNT. For bundles, the laser power levels were kept below 0.5 mW to avoid excessive heating of the DWNTs. The scattered light was collected through a 100× objective using a backscattering geometry. A Nd:YAG laser was used to generate $E_{laser}=2.33$ eV light and a Kr$^+$ ion laser generated $E_{laser}=1.92$ eV. An argon laser working in the multimode configuration (6 W) was used to pump a dye laser containing 4-dicyanomethylene-2-methyl-6-p-dimethylamino-styryl-4H-pyran, rhodamine 6G, and R560 dyes to generate a range of laser energies $E_{laser}=1.89-1.99$ eV, $E_{laser}=2.05-2.09$ eV, and $E_{laser}=2.24-2.30$ eV, respectively. To generate $E_{laser}=1.58-1.66$ eV, a Ti:sapphire laser was pumped by the argon laser. A thermoelectrically cooled Si charge coupled device detector operating at −75 °C was used to collect the Raman spectra.

III. RESULTS

A. RBM from CVD-DWNT and C_{60}-DWNT bundles

We scanned both our CVD-DWNT and C_{60}-DWNT bundled samples with 40 different laser energies (E_{laser}) ranging from 1.58 to 2.33 eV and we measured the ω_{RBM} values of each identifiable (n,m) tube. The RBM contour maps (two-dimensional color plots of the RBM intensity for ω_{RBM} vs E_{laser}) shown in Fig. 1 correspond to (a) CVD-DWNTs and (b) C_{60}-DWNTs, and both are superimposed on a SWNT-based Kataura plot of optical transition energy E_{ii} vs the frequency of the radial breathing mode.[11] The Kataura plot was calculated within the extended tight binding framework,[11] including many-body corrections, and fitted to the resonance Raman scattering data from sodium dodecyl sulfate wrapped high pressure CO conversion SWNTs.[12] A SWNT-based Kataura plot was found to be accurate enough for a qualitative identification of the (n,m) indices of the inner and outer tubes of the DWNTs. In principle, each of the four possible DWNT configurations is expected to have
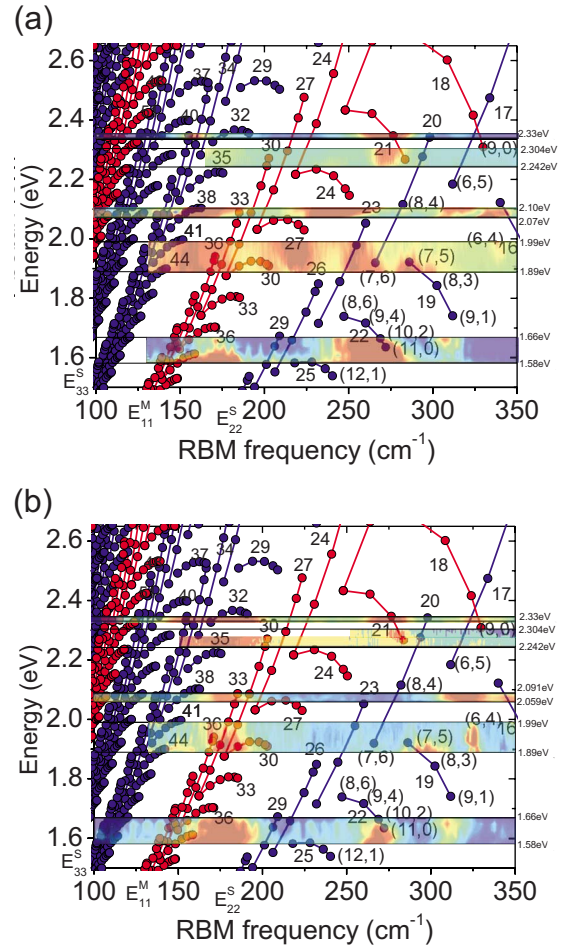

FIG. 1. (Color online) Experimental contour Raman maps of the RBM region from (a) CVD-DWNTs and (b) C_{60}-DWNTs superimposed on a Kataura plot of the resonant transition energies vs RBM frequencies for SWNTs based on the extended tight binding model (Ref. [11]). The horizontal lines mark the E_{laser} regions where Raman spectra were acquired in 5 nm intervals. In the contour Raman maps the red (blue) color corresponds to regions of maximum (minimum) Raman intensity in arbitrary units.

unique electronic and optical properties and hence to produce a unique Kataura plot. By comparing the Raman maps from CVD-DWNTs and C_{60}-DWNTs in Fig. 1, we find, in agreement with previous work,[4] a marked difference between the diameter distributions of the tubes contained in each type of sample. On one hand, the CVD-DWNT Raman map reveals the presence of inner and outer tubes whose RBMs span the entire range from 140 to 350 cm^{-1}. On the other hand, the C_{60}-DWNT RBM Raman map does not show any resonant tubes in the 190–250 cm^{-1} range but only shows outer tubes with $\omega_{RBM} < 190$ cm^{-1} and inner tubes with $\omega_{RBM} > 250$ cm^{-1} [see Fig. 1(b)]. This apparent difference in diameter distributions between CVD-DWNT and C_{60}-DWNT bundles arises from the fact that, unlike the CVD-DWNTs, where both inner and outer tubes grow simultaneously, C_{60}-DWNTs experience different diameter constraints during growth. For the case of the C_{60}-DWNTs the possible diameters of the inner tubes are constrained by the diameters of the starting SWNT material ($\sim 1.3-1.4$ nm) which forms the outer tubes of the DWNTs.

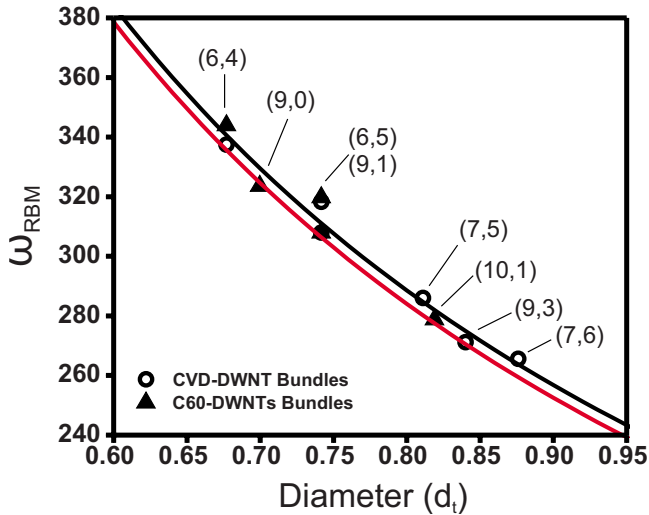FIG. 2. (Color online) (Top black line) Best fit (ω_{RBM} =228.8/d_t+2.4) to the experimental ω_{RBM} vs d_t data points from CVD-DWNTs (circles) and C$_{60}$-DWNTs (triangles). (Bottom red line) Experimental ω_{RBM} as a function of d_t for supergrowth SWNTs (ω_{RBM}=227.0/d_t+0.3) (Ref. 14).

The relationship between ω_{RBM} and d_t for the inner tubes and outer tubes of DWNTs is not expected to be the same as it would be for SWNTs with similar diameters. There are no experimental or theoretical ω_{RBM} vs d_t relationships presently available for the inner and outer tubes that constitute the four different kinds of DWNT configurations (S@S, S@M, M@S, and M@M). We thus measured the ω_{RBM} values of the identifiable (n,m) tubes in our CVD-derived and C$_{60}$-derived DWNT samples (see Fig. 2 and Table I) and found the experimental ω_{RBM} to d_t relationship of the inner tubes to be $\omega_{RBM}=A/d_t+B$, where A=228.8 cm^{-1} nm and B=2.4 cm^{-1}. For comparison, in the case of SWNTs, a proportionality constant of A=227.0 cm^{-1} nm has been reported

TABLE I. The (n,m) index and d_t with corresponding experimental ω_{RBM} from the inner tubes of CVD-DWNTs (top) and C$_{60}$-DWNTs (bottom). A horizontal line separates CVD-DWNTs (top) from C$_{60}$-DWNTs (bottom). The E_{laser} column denotes the laser energy at which the ω_{RBM} was measured (see Fig. 2).

(n,m)	d_t (nm)	ω_{RBM} (cm^{-1})	E_{laser} (eV)
(6,4)	0.67	337.4	2.080
(6,5)	0.74	318.3	2.100
(7,5)	0.81	286	1.898
(7,6)	0.87	265.6	1.898
(9,1)	0.74	308	1.668
(9,3)	0.84	271.2	2.304
(6,4)	0.67	343.9	2.059
(6,5)	0.74	319.7	2.059
(9,0)	0.69	323.6	2.333
(9,1)	0.74	307.9	1.668
(10,1)	0.81	278.8	2.304

to be the fundamental relation for pristine SWNTs in agreement with the elastic properties of graphite[13] and B =0 cm^{-1} is expected for an ideal case where the effects of the medium surrounding the nanotubes are absent (see Fig. 2). The ω_{RBM} data for our DWNTs show a slight upshift from the fundamental ω_{RBM}=227.0/d_t relation for pristine SWNTs. A list of the small diameter tubes (d_t<0.9 nm) whose (n,m) indices were unambiguously identified in the CVD-DWNT and C$_{60}$-DWNT samples is presented in Table I.

Further inspection of our DWNT bundle spectra reveals a *splitting* of the RBM from the inner tubes. The RBM splitting in DWNTs has been reported to occur when various inner tubes with a specific (n,m) are contained inside different outer tubes with various diameters and chiralities. When, for a given (n,m) inner tube, the diameter of the outer tube is decreased, the wall to wall distance decreases and the ω_{RBM} of the inner tubes upshifts.[15–18] Thus, a group of DWNTs, with the same (n,m) inner tube and different outer tubes, generates a cluster of RBM peaks and we refer to this effect above as a splitting of its ω_{RBM}.

In accordance with previous reports,[15] we observe this RBM splitting effect to be more pronounced in the C$_{60}$-DWNTs than in the CVD-DWNTs. For instance, the cluster of RBM peaks generated by the (7,5) inner tubes (see Fig. 3) in the C$_{60}$-DWNT (CVD-DWNT) bundles contains eight (five) distinguishable RBM peaks spread over a 29 (22) cm^{-1} range. However, we also find that the RBM splitting effect is not necessarily always present for the inner tubes of DWNTs. For instance, the RBMs from the (6,4) inner tubes in C$_{60}$-DWNT bundles have been reported to span over a 30 cm^{-1} range,[16] whereas in our DWNTs the RBMs from the (6,4) inner tubes for both CVD-DWNTs and C$_{60}$-DWNTs only split within a <11 cm^{-1} range [see Figs. 3(a) and 3(b)]. The small diameter (7,2) inner tube [see Fig. 3(b)] observed in the C$_{60}$-DWNTs also does not show any significant splitting. Thus, even when one would expect smaller diameter inner tubes to show increased splitting because they can fit inside a larger variety of DWNT outer tubes, energy minimizing processes that occur during sample preparation are key to defining the final (n,m) indices and wall to wall distances of the inner and outer tubes that constitute the DWNTs contained in a given sample.

Interestingly, the (7,2) inner tube does not appear in our CVD-DWNT sample [see Fig. 3(a)]. Figure 3 also shows that the inner tubes of the CVD-DWNTs have RBM peaks with larger full width at half maxima (FWHMs) than the C$_{60}$-DWNTs. This observation suggests that the phonon lifetimes in the inner tubes are longer in C$_{60}$-DWNTs than in the CVD-DWNTs. However, the intensity of the D band in C$_{60}$-DWNTs (not shown here) is greater than that in the CVD-DWNTs, indicating that the former have a larger defect concentration. In a conventional SWNT sample an increased defect concentration would be expected to give rise to more phonon relaxation pathways, decreased phonon lifetimes, and increased RBM FHWM values.[19] The fact that C$_{60}$-DWNTs show both sharper RBM peaks and higher D-band intensities than their CVD counterparts suggests that either (a) the C$_{60}$-DWNT sample contains traces of unwanted amorphous carbon or (b) the majority of the defects in the
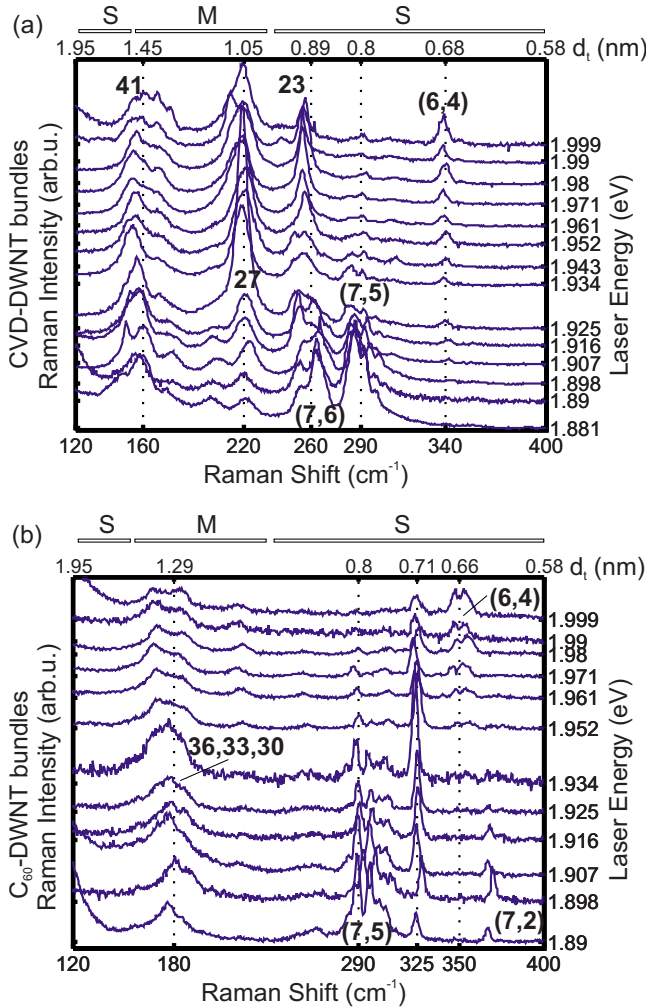
FIG. 3. (Color online) I_{RBM} vs ω_{RBM} for (a) CVD-DWNT and (b) C_{60}-DWNT bundles for the 1.89–1.999 eV E_{laser} range. The top horizontal axes mark the expected d_t (nm) of the tubes according to our experimentally obtained ω_{RBM} vs d_t relationship (ω_{RBM} =228.8/d_t+2.4 cm^{-1}). The regions marked with an M (S) correspond to metallic (semiconducting) tubes. In the cases where the exact (n,m) of the tube cannot be unambiguously identified, the $(2n+m)$ family of the corresponding group of tubes is marked.

C_{60}-DWNTs lie in the outer walls which themselves contain crystalline inner tubes that allow for long phonon lifetimes and produce the observed sharp RBM features.

Besides the above-mentioned RBM splitting caused by inner-outer tube interactions in DWNTs, a second mechanism independent of inner-outer tube interactions, known as corrugation of the inner tube, may be capable of generating extra peaks in the RBM region corresponding to the inner tubes of DWNTs. According to Muramatsu *et al.*,[20] if the fullerenes inside a SWNT are annealed at relatively low temperatures that do not provide the required thermal energy to enable complete fullerene coalescence, the resulting inner tubes will contain nonhexagonal carbon rings and have a corrugated structure. Inner tubes with a corrugated structure may show complex RBM-like vibrational modes. The presence of corrugated inner tubes in our DWNT samples is a possibility but since our sample is heat treated at a high

temperature (1700 °C), the so-called corrugation effect is weak and the inner-outer tube interaction is the dominant factor affecting the number and frequency of the observed inner-tube RBMs.

B. RBM from individual C_{60}-DWNTs

In order to investigate the DWNT configurations contained in our DWNT bundle samples, we isolated DWNTs on a Si substrate and used a Raman mapping technique[10,18] to obtain Raman resonance spectra from both the inner and outer tubes of the same individual DWNT. The individual DWNT specimens that we specially identified for this study are C_{60}-DWNTs with an S@M configuration, where the inner S tubes are either (6,5), in resonance with E_{laser} =2.10 eV, or (9,1), in resonance with E_{laser}=1.662 eV. Although the (6,5) and (9,1) tubes are both contained inside M tubes and have almost the same diameter (d_t=0.74 nm), the (6,5) tube is a type-II semiconductor and the (9,1) tube is a type-I semiconductor.[21] Since these semiconducting type-I and type-II tubes have essentially the same diameter but a different chirality dependence of E_{ii}^S,[19] we considered that the interaction between each type of inner S tube with its corresponding outer M tube may vary somewhat. Figure 4 compares the RBM regions of CVD-DWNT bundles and C_{60}-DWNT bundles with the spectra from the individual S@M C_{60}-DWNTs whose inner tubes are (9,1) type I and (6,5) type II. As expected, the peaks from the inner tubes of the individual S@M DWNT tubes can be found within the frequency region that is occupied by the broader RBM peak generated by the DWNT bundle samples (see Fig. 4).

In the case of the (6,5) type-II tube, the ω_{RBM} from the individual tubes can be found in the 313–329 cm^{-1} range where the highest RBM frequencies correspond to tubes that are paired with the smallest diameter outer tubes.[16,18] In the case of the (9,1) inner tubes, the ω_{RBM}'s for the two specimens were found to appear in the 311–316 cm^{-1} range. Similarly, the ω_{RBM}'s for the outer tubes pairing with the (6,5) tubes appear in the 175–168 cm^{-1} range, and the outer tubes pairing with the two (9,1) tubes appear close to 173 cm^{-1}. If we use ω_{RBM}=228.8/d_t+2.4 cm^{-1} to approximate the wall to wall distance in our individual S@M DWNTs, the specimens with type-I and type-II inner tubes would both have nominal wall to wall distances (in the 0.29–0.32 nm range) that are 5–15 % smaller than the interlayer spacing in graphite (0.34 nm). This unexpected result stems from the lack of a $\omega_{RBM}(d_t)$ relationship capable of taking into account other effects that affect the ω_{RBM} such as the M/S configuration of the DWNT, the intertube stress on the outer tube, the substrate, and the adsorbed species on the outer tube's wall. Nevertheless, even if we cannot obtain a direct measurement of the actual wall to wall distance, we observe that the d_t dependence of the ω_{RBM} from the inner and outer tubes of an S@M DWNT is similar to within our experimental error regardless of whether the inner semiconducting tube is type I or type II. We were not able to obtain an (n,m) assignment for the outer tubes from our spectra because the E_{ii}'s from other tubes with similar diameters were too close to each other in energy (see Fig. 1). However,
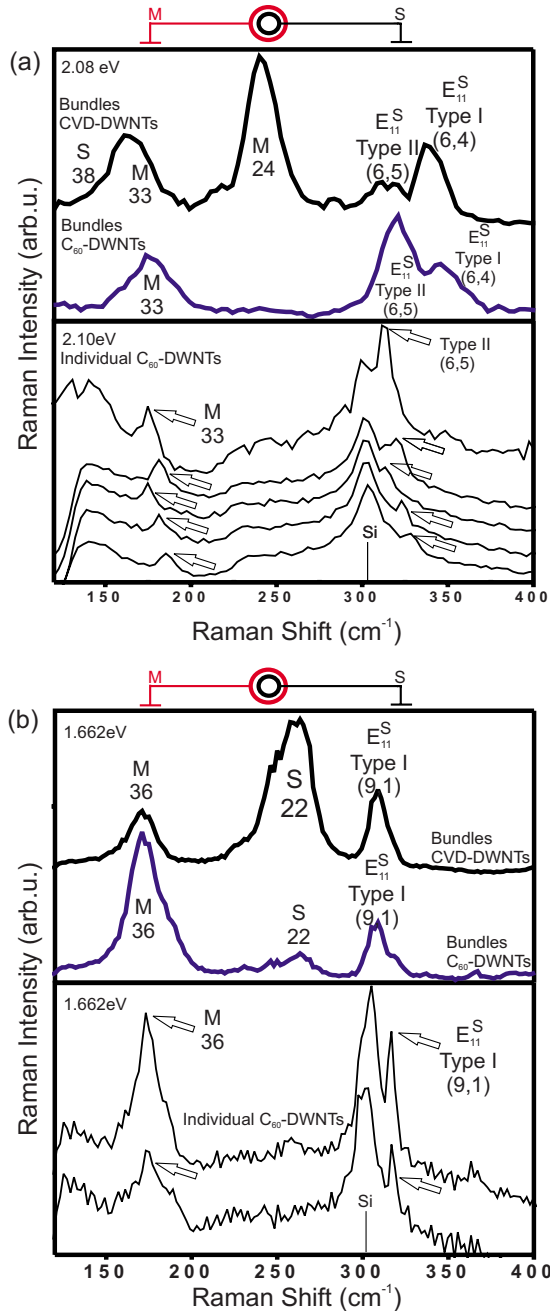
FIG. 4. (Color online) (a) I_{RBM} vs ω_{RBM} from CVD-DWNT bundles, C_{60}-DWNT bundles, and five individual C_{60}-DWNTs (marked by arrows pointing at the inner and outer tube pairs) for similar E_{laser} (2.08 and 2.10 eV) excitation energies that excite DWNTs with the S@M configuration. The individual DWNTs have inner tubes that are (6,5) type-II S tubes paired with outer M tubes belonging to $(2n+m)$ family 33. (b) I_{RBM} vs ω_{RBM} from CVD-DWNTs bundles, C_{60}-DWNT bundles, and two individual C_{60}-DWNTs using $E_{laser}=1.662$ eV. The individual S@M DWNTs (marked by arrows pointing at the inner and outer tube pairs) have inner tubes that are (9,1) type-I S tubes paired with outer M tubes belonging to $(2n+m)$ family 36.

the data are sufficiently accurate to tell us that the outer tubes of the individual DWNTs with inner (6,5) and (9,1) tubes belong to $(2n+m)$ families 33 and 36, respectively.

C. G band from CVD-DWNT and C_{60}-DWNT bundles

The G band is generated by in-plane C-C bond stretching modes that occur in the form of optical phonons along the axial [longitudinal optical (LO) mode] and circumferential [transverse optical (TO) mode] directions of a carbon nanotube.[19] In metallic (semiconducting) tubes, the G^- and G^+ features originate from the LO (TO) and TO (LO) phonons, respectively.[22] Since the curvature in a nanotube weakens the bonds in the circumferential direction, the $\omega_{G_{TO}}$ downshifts with decreasing nanotube diameter.

By measuring the Raman spectra from our DWNTs in the $E_{laser}=1.58-2.33$ eV range (see Fig. 5), we scanned across regions of the resonance windows of the inner and outer tubes that belong to DWNTs with the four possible configurations mentioned above. The inner and outer tubes of the same DWNT are not necessarily in resonance with the same E_{laser}. However, if the RBM and G-band resonance windows of a certain inner tube are centered at roughly the same energy, we can assume, for a certain E_{laser}, that the observed line shape of the G band is predominantly generated by those tubes that show a resonant RBM signal. We can thus analyze the RBM region of a spectrum, relate it to its corresponding G-band region, and assume that the tubes with RBMs which are in resonance with a given E_{laser} have a predominant effect on the observed line shape of the G band.

In the $E_{laser}=1.58-1.99$ eV range for CVD-DWNTs, we observe that the inner tubes in resonance are predominantly semiconducting (S@S and S@M) [see Fig. 1(a)]. In this case, the frequencies of the G^+ band (ω_{G^+}) are centered around 1588 cm^{-1} with a full width at half maximum intensity of FWHM$_{G^+}\approx15$ cm^{-1} [see Fig. 5(a)] and $\omega_{G^-}\approx1555$ cm^{-1} with FWHM$_{G^-}\approx42$ cm^{-1}. The presence of the outer M tubes is likely to be contributing to the large FWHM of ω_{G^-}. On the other hand, for $E_{laser}\geq2.07$ eV, besides being in resonance with S@S and S@M CVD-DWNTs, we also find resonance with CVD-DWNTs having inner metallic tubes (M@S and M@M) that belong to $(2n+m)$ families 24 and 21 [see Fig. 1(a)] and we observe that the line shape of the G band undergoes a series of noticeable changes [see Fig. 5(a)] as E_{laser} is increased. These changes in the G-band line shape, which coincide with the appearance of the resonance with M inner tubes, are (a) an ω_{G^+} upshift of ~7 cm^{-1} (from $\omega_{G^+}\approx1588$ cm^{-1} at 1.581 eV to $\omega_{G^+}\approx1595$ cm^{-1} at 2.33 eV), (b) an ~16 cm^{-1} splitting of the G^+ band and G^- band ($\omega_{G^-}\approx1580$ cm^{-1} and $\omega_{G^+}\approx1595$ cm^{-1} at 2.33 eV), and (c) an ~6 cm^{-1} increase in FWHM$_{G^+}$ (from FWHM$_{G^+}\approx15$ cm^{-1} at 1.581 eV to FWHM$_{G^+}\approx21$ cm^{-1} at 2.33 eV). The above-mentioned changes can be appreciated in Fig. 5(c), where spectra for the two extrema in E_{laser} are shown (predominant resonance with S@S and S@M DWNTs at $E_{laser}=1.581$ eV to be compared with the resonance with M@S and M@M DWNTs at $E_{laser}=2.33$ eV).

In the case of C_{60}-DWNTs, the distribution of the four possible DWNT configurations present in the sample is different and we do not find a strong resonance with inner M tubes belonging to the $(2n+m)$ family 24 for $E_{laser}=2.242-2.304$ eV [see Fig. 5(b)]. Instead we only find strong resonance with inner M tubes for $E_{laser}=2.33$ eV which excites (9,3) inner M tubes belonging to family 21.
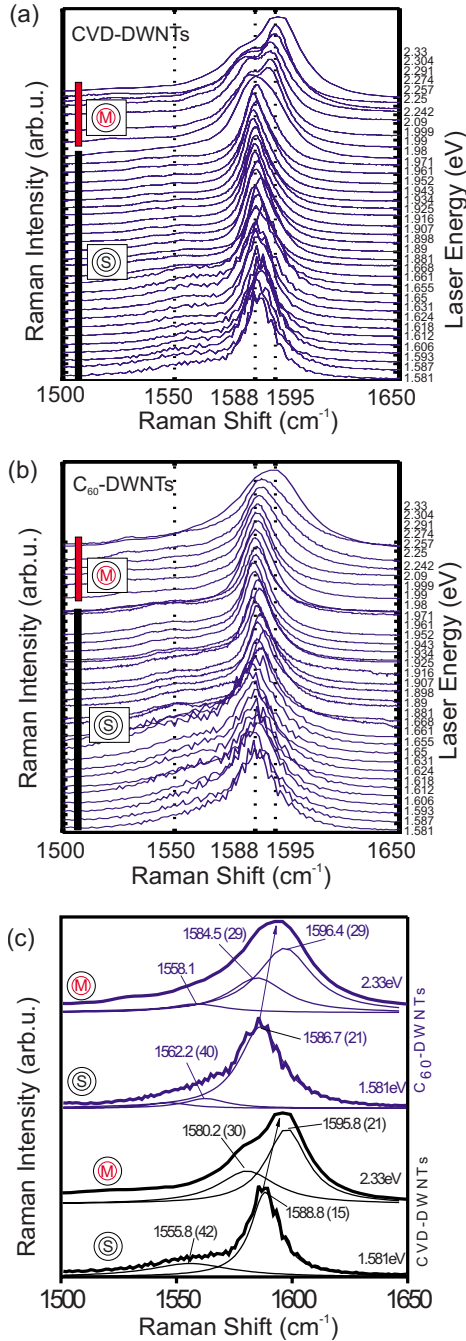
FIG. 5. (Color online) Raman G-band intensity I_G vs ω_G for the 1.581–2.33 eV E_{laser} range from (a) CVD-DWNT bundles and (b) C_{60}-DWNT bundles. The dark vertical lines on the left mark the energy regions where the inner tubes in resonance with E_{laser} are either predominantly semiconducting (E_{laser}=1.581–1.999 eV resonant with S@S or S@M) or predominantly metallic (E_{laser}=2.09–2.33 eV resonant with M@S or M@M). (c) The G-band from C_{60}-DWNT bundles (top) and CVD-DWNT bundles (bottom) for E_{laser} excitation energies that predominantly resonate with either inner semiconducting tubes (E_{laser}=1.581 eV, S@S or S@M) or inner metallic tubes (E_{laser}=2.33 eV, M@S or M@M).

The line shape of the G band for C_{60}-DWNTs is similar for all excitation energies in the $E_{laser} < 2.33$ eV range where mostly DWNTs with S inner tubes are excited. However,

when E_{laser}=2.33 eV is reached and DWNTs with inner M tubes are excited [see Fig. 5(c)], the G band upshifts (~ 9 cm^{-1} increase in ω_{G+}), splits (~ 12 cm^{-1} separation between ω_{G-} and ω_{G+}), and broadens (~ 8 cm^{-1} increase in FWHM). The upshift and broadening of ω_{G+} when in resonance with M@S and M@M DWNTs is consistently observed in both the CVD-DWNTs and C_{60}-DWNTs. Therefore, in DWNT bundles, the line shape of the G band is not only dependent on the sample's diameter distribution but also on its DWNT M/S configuration distributions.

D. G′ band from CVD-DWNT and C_{60}-DWNT bundles

The G′ band is based on a two-phonon intervalley double resonance process that does not require the presence of defects.[23] In general, the G′ band is generated by four steps where (a) an incoming photon excites an electron with wave vector **k**, (b) the electron is scattered from **k** to **k**+**q** by emitting a phonon with wave vector **q**, (c) the electron is backscattered from **k**+**q** to **k** by emitting a second phonon, and (d) the electron recombines with a hole at **k**.[24] Since the laser excitation energy (E_{laser}) determines the **k** of the excited electron and the **q** of the emitted phonons, the G′-band mode is dispersive.[25] For reference, in SWNTs the reported dispersion of the G′-band feature is ~ 106 cm^{-1}/eV.[19] Also, like other Raman modes, the G′ band has a diameter dependence.

In DWNT bundles, the diameter distribution is bimodal and we expect a G′ band with two main features that correspond to the inner (G'_1) and outer (G'_2) tubes.[26] The intensity ($I_{G'}$), the absolute frequency ($\omega_{G'}$), the dispersion ($\partial \omega_{G'} / \partial E_{laser}$), and the FWHM (FWHM$_{G'}$) linewidth of the two G′-band components in DWNTs are dependent on nanotube diameter, chirality, metallicity, and other factors, such as doping, strain, and energy of the incoming photons. Figure 6 shows $I_{G'}$ vs $\omega_{G'}$ from (a) CVD-DWNT bundles and (b) C_{60}-DWNT bundles for the 1.881–2.33 eV E_{laser} range. The CVD-DWNT sample shows a two peaked structure where the low frequency peak (G'_1), which corresponds to the inner tubes,[26,27] has a higher intensity than its higher frequency counterpart (G'_2). The $I_{G'_1/G'_2}$ and FWHM$_{G'_1/G'_2}$ ratios (not presented here) show a tendency to increase with increasing E_{laser}. Interestingly, the dispersion of the peak corresponding to the inner tubes ($\partial \omega_{G'_1} / \partial E_{laser}$=122.21 cm^{-1}/eV) is considerably larger than that of the outer tubes ($\partial \omega_{G'_2} / \partial E_{laser}$ =89.44 cm^{-1}/eV), indicating that the inner and outer tubes, which vary in diameter and chirality, possess different sets of $E(\mathbf{k})$ dispersion relations with different slopes and thus enable the selection of different **q** wave vectors [see Fig. 6(c)]. The inherent difference between the phonon dispersion relations of the inner and outer tubes also contributes to the final $\partial \omega_{G'} / \partial E_{laser}$ values of the G′1 and G′2 features.

The G′-band spectra from the C_{60}-DWNTs also has a two peaked structure where the intensity of G'_1 relative to G'_2 tends to increase with increasing E_{laser}. Interestingly, we observe a slight downshift in the frequency of the G′ band of C_{60}-DWNTs with respect to CVD-DWNTs for spectra taken at the same E_{laser}. In particular, the $\omega_{G'_2}$ of the C_{60}-DWNTs is on average ~ 6.5 cm^{-1} below its CVD-derived counterpart
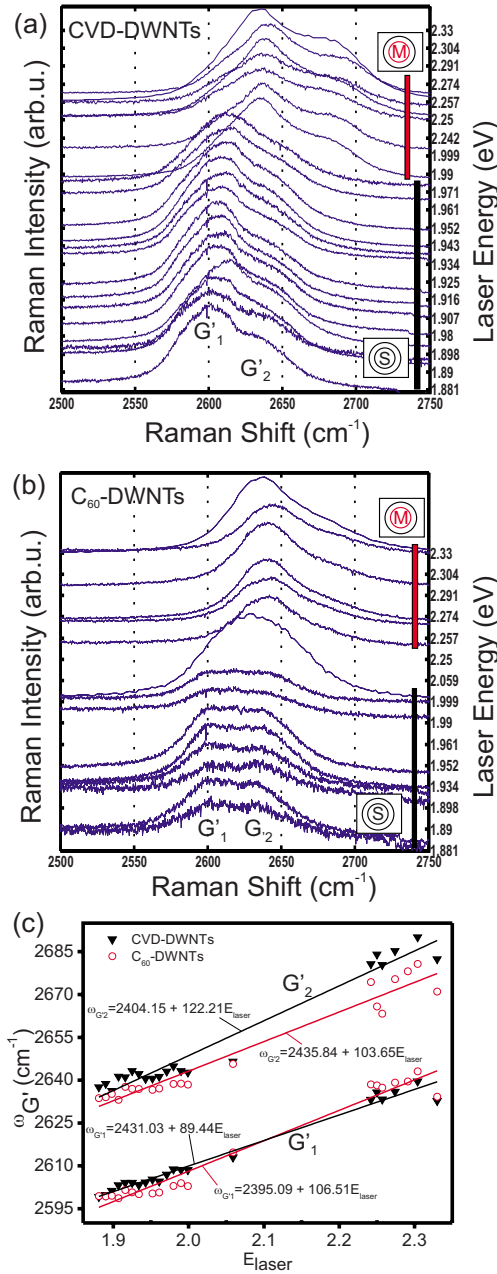
FIG. 6. (Color online) The I_G vs $\omega_{G'}$ from (a) CVD-DWNT bundles and (b) C_{60}-DWNT bundles for the 1.881–2.33 eV E_{laser} range. The dark vertical lines on the right mark the energy regions where the inner tubes in resonance with E_{laser} are either predominantly semiconducting ($E_{laser} < 2.2$ eV resonant with S@S or S@M) or predominantly metallic ($E_{laser} > 2.2$ eV resonant with M@S or M@M). (c) The dispersion of the low ($\omega_{G'_1}$) and high ($\omega_{G'_2}$) frequency components of the G′ band from CVD-DWNT bundles (triangles) and C_{60}-DWNT bundles (circles).

[see Fig. 6(c)]. Similarly, $\omega_{G'_1}$ is on average 3.4 cm^{-1} below its CVD counterpart for $E_{laser} < 2$ eV. This observation is consistent with the fact that $\omega_{G'}$ scales directly with tube diameter[19] because the average diameter of the SWNTs that were used to fabricate our C_{60}-DWNTs is likely to be smaller than the outer tube diameters that are present in the CVD-DWNT sample. In C_{60}-DWNTs the dispersions of G'_1

($\partial\omega_{G'_1}/\partial E_{laser} = 106.51$ cm^{-1}/eV) and G'_2 ($\partial\omega_{G'_2}/\partial E_{laser}$ $= 103.65$ cm^{-1}/eV) are similar and the difference between them (~ 3 cm^{-1}/eV) is smaller than the difference between $\partial\omega_{G'_1}/\partial E_{laser}$ and $\partial\omega_{G'_2}/\partial E_{laser}$ observed in the CVD-DWNTs (~ 30 cm^{-1}/eV). The fact that the diameter distribution of the inner and outer tubes is narrower in the C_{60}-DWNTs than in the CVD-DWNTs is one of the possible causes for the differences between $\partial\omega_{G'_1}/\partial E_{laser}$ and $\partial\omega_{G'_2}/\partial E_{laser}$ being smaller in C_{60}-DWNTs than in CVD-DWNTs.

From previous experiments performed on SWNTs, the $\omega_{G'}$ was found to have a d_t dependence of the form $\omega_{G'} = \omega_0 + \beta/d_t$, where $\omega_0 = 2704$ cm^{-1} and $\beta = -35.4$ cm^{-1} nm for $E_{laser} = 2.41$ eV.[19] However, the inner tubes from both CVD-DWNT and C_{60}-DWNT bundled samples show deviations from the above-mentioned SWNT-based $\omega_{G'}(d_t)$ relation. The SWNT-based $\omega_{G'}(d_t)$ relation predicts that our inner tubes with diameters in the 0.7–0.9 nm range should have $\omega_{G'_1}$ in the 2653–2664 cm^{-1} range. However, for the CVD-DWNT (C_{60}-DWNT) sample at $E_{laser} = 2.33$ eV, $\omega_{G'_1}$ $= 2632$ cm^{-1} ($\omega_{G'_1} = 2634$ cm^{-1}) which is in both cases below the SWNT-based prediction.

In the case of the outer tubes, there is reasonably good agreement with the SWNT-based $\omega_{G'}(d_t)$ relation. The SWNT-based relation predicts $\omega_{G'}$ to be in the 2676–2681 cm^{-1} range for tubes with d_t in the 1.3–1.6 nm range and we measure $\omega_{G'_2} = 2682$ cm^{-1} ($\omega_{G'_2} = 2671$ cm^{-1}) for the CVD-DWNTs (C_{60}-DWNTs). In agreement with previous reports,[26] the SWNT-based $\omega_{G'}(d_t)$ relation may predict the $\omega_{G'}$ of the outer tubes quite well but it cannot be applied to the inner tubes because this relation does not take into account the high curvature of tubes with $d_t < 1$ nm and the possible interactions of the inner tubes with the surrounding outer tubes due to strain and electrostatic effects.

Finally, another factor that affects the lines shape of the G′ band is the distribution of the M/S configurations present in a DWNT bundle sample. In SWNTs the G′-band intensity ($I_{G'}$) has been reported to be larger for M than for S nanotubes because the electron-phonon matrix elements for the TO phonon at the K point are larger for M tubes.[28] Therefore, it is reasonable to expect that the relative intensities of G'_1 and G'_2 also depend on whether the inner and outer tubes of a DWNTs are M or S. When taking the metallicity factor into account, one must also keep in mind that the resonance window of the G′ band is wider than the resonance window of the RBM and therefore other tubes that are not in resonance with the laser excitation energy for the RBM feature can also contribute to the line shape of the G′ band. Resonance with scattered photons can also occur. Nevertheless, if we assume that both the G′ band and the RBM resonance windows of a carbon nanotube are centered around the same energy, it is reasonable to expect that the major contribution to the line shape of the G′ band in DWNTs comes from the inner and outer tubes that are in resonance with the laser excitation energy. In this context, we divide our G′-band measurements into two regimes: (I) for all $E_{lasers} > 2.2$ eV that excite M@S DWNTs and the inner M tubes of M@M DWNTs and (II) for all $E_{lasers} < 2.2$ eV that excite S@M DWNTs and the inner S tubes of S@S DWNTs (see Figs. 1 and 6). In both

C_{60}-DWNTs and CVD-DWNTs we observe that the $I_{G_1'/G_2'}$ is greater in regime II than in regime I in part because the laser energy is in resonance with the E_{11} transition of the inner M tubes. Thus, when the inner tubes in resonance with E_{laser} are predominantly metallic, we observe an enhancement of the intensity of the lower frequency G_1' region with respect to its high frequency G_2' counterpart. Experiments at the individual DWNT level may enable quantitative measurements capable of decoupling the individual contributions to the line shape of the G' band for each of the above-mentioned factors.

IV. CONCLUSIONS

By scanning a large number of laser energies we have measured the Raman spectra from CVD-derived and C_{60}-derived double-wall carbon nanotubes with the four possible metallic and semiconducting configurations. For small diameter nanotubes (<0.9 nm), the separation between the E_{ii} is large enough to allow for an accurate (n,m) identification of the inner tubes. Once the (n,m) indices of the observed inner tubes were assigned, we measured their ω_{RBM} and obtained an ω_{RBM} to d_t relationship of the form $\omega_{RBM} = A/d_t + B$. The values of the A and B constants are close to those previously obtained from the elastic properties of graphite,[13] indicating that the inner tubes are effectively shielded from the environment by their surrounding outer tubes. By scanning the RBM region from the CVD-DWNTs and C_{60}-DWNTs bundles we find that the splitting effect of the ω_{RBM} described above is not necessarily always present for all inner tubes. For the same (n,m) inner tubes, the RBM splitting behavior is observed to vary between CVD-derived and C_{60}-derived DWNTs, indicating that the energy minimizing processes inherent to each sample's synthesis method define the final $(n,m)@(n',m')$ combinations and wall to wall distances found in DWNTs. We also analyzed the Raman spectra from individual S@M DWNTs with inner (6,5) type-II and (9,1) type-I semiconducting tubes. The upshift in the ω_{RBM} of the inner tube caused by a decrease in the diameter of the outer tube was observed to follow the same trend in both type-I (6,5) and type-II (9,1) inner semiconducting tubes. The line shape and frequency of the G band from CVD-DWNT and C_{60}-DWNT bundles were analyzed using various laser excitation energies and changes in the G-band line shape were correlated with a switch in resonance for DWNTs whose inner tubes are predominantly semiconducting (S@S and S@M) to resonance with DWNTs with predominantly inner metallic tubes (M@M and M@S). Finally, the G'-band frequency of C_{60}-DWNT bundles is observed to be downshifted with respect to that of CVD-DWNTs due to differences in the diameter distributions and M/S configuration populations of the samples.

[1] M. Endo, H. Muramatsu, T. Hayashi, Y. A. Kim, M. Terrones, and N. S. Dresselhaus, Nature (London) **433**, 476 (2005).

[2] S. Bandow, M. Takizawa, H. Kato, T. Okazaki, H. Shinohara, and S. Iijima, Chem. Phys. Lett. **347**, 23 (2001).

[3] S. Bandow, T. Hiraoka, T. Yumura, K. Hirahara, H. Shinohara, and S. Iijima, Chem. Phys. Lett. **384**, 320 (2004).

[4] R. Pfeiffer *et al.*, Phys. Status Solidi B **245**, 1943 (2008).

[5] D. Shimamoto, H. Muramatsu, T. Hayashi, Y. A. Kim, M. Endo, J. S. Park, R. Saito, M. Terrones, and M. S. Dresselhaus, Appl. Phys. Lett. **94**, 083106 (2009).

[6] T. Okazaki, S. Bandow, G. Tamura, Y. Fujita, K. Iakoubovskii, S. Kazaoui, N. Minami, T. Saito, K. Suenaga, and S. Iijima, Phys. Rev. B **74**, 153404 (2006).

[7] M. Endo, Y. A. Kim, T. Hayashi, H. Muramatsu, M. Terrones, R. Saito, F. Villalpando-Paez, S. G. Chou, and M. S. Dresselhaus, Small **2**, 1031 (2006).

[8] Y. A. Kim, H. Muramatsu, T. Hayashi, M. Endo, M. Terrones, and M. S. Dresselhaus, Chem. Vap. Deposition **12**, 327 (2006).

[9] Y. Kim, H. Muramatsu, M. Kojima, T. Hayashi, M. Endo, M. Terrones, and M. Dresselhaus, Chem. Phys. Lett. **420**, 377 (2006).

[10] F. Villalpando-Paez *et al.*, Nano Lett. **8**, 3879 (2008).

[11] G. G. Samsonidze, R. Saito, N. Kobayashi, A. Gruneis, J. Jiang, A. Jorio, S. G. Chou, G. Dresselhaus, and M. S. Dresselhaus, Appl. Phys. Lett. **85**, 5703 (2004).

[12] A. Jorio, C. Fantini, M. A. Pimenta, R. B. Capaz, G. G. Samsonidze, G. Dresselhaus, M. S. Dresselhaus, J. Jiang, N. Kobayashi, A. Gruneis, and R. Saito, Phys. Rev. B **71**, 075401 (2005).

[13] G. D. Mahan, Phys. Rev. B **65**, 235402 (2002).

[14] P. Araujo and A. Jorio, Phys. Status Solidi B **245**, 2201 (2008).

[15] R. Pfeiffer, C. Kramberger, F. Simon, H. Kuzmany, V. N. Popov, and H. Kataura, Eur. Phys. J. B **42**, 345 (2004).

[16] R. Pfeiffer, F. Simon, H. Kuzmany, and V. N. Popov, Phys. Rev. B **72**, 161404 (2005).

[17] R. Pfeiffer, F. Simon, H. Kuzmany, V. N. Popov, V. Zolyomi, and J. Kurti, Phys. Status Solidi B **243**, 3268 (2006).

[18] F. Villalpando-Paez, H. Muramatsu, Y. A. Kim, H. Farhat,

M. Endo, M. Terrones, and M. S. Dresselhaus, Nanoscale, **2**, 406 (2010).

[19] M. Dresselhaus, G. Dresselhaus, R. Saito, and A. Jorio, Phys. Rep. **409**, 47 (2005).

[20] H. Muramatsu, T. Hayashi, Y. A. Kim, D. Shimamoto, M. Endo, V. Meunier, B. G. Sumpter, M. Terrones, and M. S. Dresselhaus, Small **5**, 2678 (2009).

[21] M. J. O'Connell *et al.*, Science **297**, 593 (2002).

[22] S. Piscanec, M. Lazzeri, J. Robertson, A. C. Ferrari, and F. Mauri, Phys. Rev. B **75**, 035427 (2007).

[23] R. Saito, A. Jorio, A. Souza Filho, A. Grueneis, M. A. Pimenta, G. Dresselhaus, and M. Dresselhaus, Physica B **323**, 100 (2002).

[24] R. Saito, A. Grüneis, G. G. Samsonidze, V. W. Brar, G. Dresselhaus, M. S. Dresselhaus, A. Jorio, C. Fantini, M. A. Pimenta, and A. G. S. Filho, New J. Phys. **5**, 157 (2003).

[25] R. Saito, A. Jorio, A. G. S. Filho, G. Dresselhaus, M. S. Dresselhaus, and M. A. Pimenta, Phys. Rev. Lett. **88**, 027401 (2002).

[26] R. Pfeiffer, H. Kuzmany, F. Simon, S. N. Bokova, and E. Obraztsova, Phys. Rev. B **71**, 155409 (2005).

[27] E. B. Barros *et al.*, Phys. Rev. B **76**, 045425 (2007).

[28] K. K. Kim, J. S. Park, S. Kim, H. Z. Geng, H. K. An, C. Yang, K. Sato, R. Saito, and Y. Lee, Phys. Rev. B **76**, 205426 (2007).